Cell, Vol. 119, 491–502, November 12, 2004, Copyright ©2004 by Cell Press

She2p Is a Novel RNA Binding Protein with a Basic Helical Hairpin Motif

Dierk Niessing,[1,4] Stefan Hüttelmaier,[3] Daniel Zenklusen,[3] Robert H. Singer,[3] and Stephen K. Burley[1,2,4,*]
[1]Laboratories of Molecular Biophysics and
[2]Howard Hughes Medical Institute
The Rockefeller University
1230 York Avenue
New York, New York 10021
[3]Department of Anatomy and Structural Biology
Albert Einstein College of Medicine
1300 Morris Park Avenue
Bronx, New York 10461

Summary

Selective transport of mRNAs in ribonucleoprotein particles (mRNP) ensures asymmetric distribution of information within and among eukaryotic cells. Actin-dependent transport of *ASH1* mRNA in yeast represents one of the best-characterized examples of mRNP translocation. Formation of the *ASH1* mRNP requires recognition of zip code elements by the RNA binding protein She2p. We determined the X-ray structure of She2p at 1.95 Å resolution. She2p is a member of a previously unknown class of nucleic acid binding proteins, composed of a single globular domain with a five α helix bundle that forms a symmetric homodimer. After demonstrating potent, dimer-dependent RNA binding in vitro, we mapped the RNA binding surface of She2p to a basic helical hairpin in vitro and in vivo and present a mechanism for mRNA-dependent initiation of *ASH1* mRNP complex assembly.

Introduction

In eukaryotic cells, mRNA translocation is required for asymmetric propagation of information (reviewed in Farina and Singer [2002], Kloc et al. [2002], Lopez de Heredia and Jansen [2004], St Johnston [1995]) and represents a central mechanism for such diverse functions as cell-to-cell communication in plants (reviewed in Ding et al. [2003]), budding of yeast (reviewed in Chartrand et al. [2001], Darzacq et al. [2003]), development of body axes in metazoans (reviewed in Mohr and Richter [2001], Wickens et al. [2000]), synaptic plasticity (reviewed in Steward and Worley [2001]), and basal-apical cell polarity (reviewed in Lopez de Heredia and Jansen [2004], Tekotte and Davis [2002]). Messenger RNAs destined for translocation are usually bound by specialized proteins and packaged into larger messenger ribonucleoprotein particles (mRNP), also known as translocons, or locasomes (Bertrand et al., 1998). Within such translocons are motor proteins, which facilitate cargo-specific transport along cellular actin or microtubule networks (reviewed in Tekotte and Davis [2002], Vale [2003]). Selective translocation and localization of *ASH1* mRNA during the budding of *Saccharomyces cerevisiae* represents one of the best-characterized examples of mRNA translocation (reviewed in Chartrand et al. [2001], Darzacq et al. [2003]).

Upon nutrient deprivation, diploid *S. cerevisiae* cells undergo meiosis, which results in four haploid spores, two pairs belonging to each opposite mating type. Only cells of opposing mating type are able to mate and form a diploid cell. To ensure that cells within a population are equally distributed between the two mating types, and, thus, capable of reproduction, the mother cell but not the daughter cell switches its mating type after each cell division (reviewed in Chartrand et al. [2001], Darzacq et al. [2003]). Yeast regulates mating-type switching by inhibiting expression of HO endonuclease in daughter cells via specific transcriptional repression of HO endonuclease (Ash1p). Exclusive daughter cell expression of Ash1p is achieved by active localization of *ASH1* mRNA to the bud tip of the daughter cell (Long et al., 1997; Takizawa et al., 1997). At the bud tip, the mRNA is translated into Ash1p, which represses transcription of the inducer of mating-type switch (i.e., the HO endonuclease; Bobola et al., 1996; Sil and Herskowitz, 1996).

Genetic screening has identified three core components of the *ASH1* mRNA translocation complex, including She1p/Myo4p, She2p, and She3p (Jansen et al., 1996). She1p/Myo4p is a type V unconventional myosin that conveys *ASH1* mRNA-containing RNPs along the actin network (Bertrand et al., 1998; Bobola et al., 1996; Jansen et al., 1996; Long et al., 1997; Münchow et al., 1999; Reck-Peterson et al., 2001; Takizawa et al., 1997). She2p facilitates *ASH1* mRNA binding by recognizing four independent zip code elements (Böhl et al., 2000; Chartrand et al., 1999, 2002; Gonzalez et al., 1999; Long et al., 2000). Myo4p and She2p are connected by the adaptor protein She3p (Böhl et al., 2000; Long et al., 2000; Münchow et al., 1999; Takizawa and Vale, 2000). A recently published study showed that the Pumilio family protein Puf6p, which is not deemed to be part of the core translocation machinery, associates with the *ASH1* mRNP complex to repress translation of *ASH1* mRNA during translocation (Gu et al., 2004).

As in the paradigm common to metazoans (reviewed in Dreyfuss et al. [2002], Kloc et al. [2002]), She2p may escort *ASH1* mRNA from the nucleus, during translocation as part of a translationally silent mRNP, until *ASH1* mRNA is anchored at its target site (Bertrand et al., 1998; Böhl et al., 2000; Kruse et al., 2002; Takizawa and Vale, 2000). After translocation into the cytoplasm, the adaptor protein She3p binds the She2:*ASH1* mRNA complex. Together with She1p/Myo4p, the complex assembles into a larger mRNP (Long et al., 2000; Takizawa and Vale, 2000). Thereafter, the *ASH1* mRNP is transported into the bud and translation is activated.

Despite significant progress in identifying and characterizing a large number of RNA binding motifs (reviewed in Dreyfuss et al. [2002]), unsuccessful attempts to detect similarity between the amino acid sequence of

*Correspondence: sburley@stromix.com
[4]Present address: Structural GenomiX, Inc., 10505 Roselle Street, San Diego, California 92121.

She2p and the amino acid sequences of known RNA binding proteins (Böhl et al., 2000; Gonsalvez et al., 2003; Long et al., 2000) suggest that it does not belong to any previously identified class of RNA binding proteins. Attempts to use comparative protein structure modeling (Pieper et al., 2004) to predict its three-dimensional structure were similarly unsuccessful (data not shown).

We used X-ray crystallography to determine the three-dimensional structure of She2p at 1.95 Å resolution, which revealed that the She2p polypeptide chain folds into a single globular domain consisting of a bundle of five antiparallel α helices with a small additional helix protruding at right angles from the middle of the bundle. She2p forms a stable dimer that is required for function in vitro and in vivo. Systematic comparison with previously determined structures available in the Protein Data Bank (PDB, http://www.rcsb.org/pdb/) revealed no similarity between She2p and known nucleic acid binding proteins. We determined that She2p binds its target mRNA with high affinity in vitro, mapped the RNA binding surface of She2p in vitro and in vivo, and present a molecular mechanism for RNA-dependent initiation of the assembly of *ASH1* mRNP complex.

Results

Structure Determination

Initial poor-quality crystals were obtained from recombinant full-length She2p expressed in *E. coli*. Results of limited proteolysis combined with matrix-assisted laser desorption/ionization mass spectrometry (MALDI-MS) suggested that N- and C-terminal segments of the She2p polypeptide chain do not adopt stable secondary structures. A total of 20 different N- and/or C-terminal truncations of She2p with various additional amino acid alterations were expressed in *E. coli*, purified to homogeneity, and used in crystallization trials (see Experimental Procedures). Diffraction-quality crystals were obtained from a truncated form of She2p (residues 6–239) with all four Cys residues (Cys14, Cys68, Cys106, and Cys180) changed to serine to overcome oxidation during purification. The X-ray crystal structure was determined via multiple isomorphous replacement (Table 1; Ke, 1997). The final refinement model was obtained at 1.95 Å resolution, with excellent crystallographic statistics (R_{work} = 19.1%, R_{free} = 24.1%; Brünger, 1992) and stereochemistry (see Table 1 and Experimental Procedures for a complete description of structure determination and refinement).

She2p Is a Symmetric Homodimer

The She2p polypeptide chain folds into a single domain consisting of a bundle of five antiparallel α helices (monomer dimensions: 70 Å × 30 Å × 45 Å; Figure 1), which are arrayed like a pentacle around a central axis and contribute stacking aromatic side chains to the hydrophobic core. A small additional α helix protrudes at right angles from the middle of the bundle. Within the crystal, She2p forms a noncrystallographic dimer (dimensions: 70 Å × 54 Å × 62 Å), stabilized by significant buried solvent-accessible surface area (~2015 Å^2/monomer) and several hydrophobic amino acids contributing to the dimer interface. The two halves of the dimer are symmetric, with their pentacle bundles superimposing with a root-mean-square deviation (rmsd) of 0.43 Å (for 141 common α carbon atom pairs). The atomic model of the first monomer lacks residues 184–191 and 238–239, whereas, in the second monomer, residues 6–12, 77–91, 178–203, and 238–239 are missing (residues 1–5 and 240–246 were excluded from the expression construct, see Experimental Procedures).

Within the crystal, we observed a dimer-dimer contact with buried solvent-accessible surface area of 663 Å^2/dimer, which is significantly smaller than interfaces reported for most stable oligomers (Conte et al., 1999; Dasgupta et al., 1997). Size exclusion chromatography suggested that She2p oligomerizes in solution, and analytical equilibrium ultracentrifugation revealed the predominant She2p-oligomerization state at concentrations of 8–32 μM to be dimeric (data not shown; see Experimental Procedures). Point mutations predicted to interfere with potential tetramer formation in solution did not result in a change in size exclusion chromatography behavior and did not affect RNA binding (data not shown). We conclude, therefore, that the observed She2p dimer-dimer contact in the crystal is almost certainly not of physiologic importance.

She2p Represents a Novel Protein Fold

Systematic comparison of She2p with structures previously deposited in the PDB using the DALI server (Holm and Sander, 1998) revealed no detectable similarity to known nucleic acid binding proteins. Instead, the α helix core of She2p bears some resemblance to the central domain of fumarase/aspartase homologous superfamily members (CATH-ID, 1.20.200.10), including fumarase C (PDB ID, 1fur-A; Z score, 8.6; rmsd = 4.2 Å for 169 α carbon pairs), adenylosuccinate lyase (PDB ID, 1c3c-A; Z score, 7.7; rmsd = 3.9 Å for 170 α carbon pairs), the eye lens protein δ-2 crystallin (PDB ID, 1auw-A; Z score, 7.7; rmsd = 4.0 Å for 172 α carbon pairs), and β-carboxy-*cis*, cis-muconate cycloisomerase (PDB ID, 1q5n; Z score, 7.6; rmsd = 4.3 Å for 178 α carbon pairs). Although class II fumarases like fumarase C oligomerize via their central domain (Weaver et al., 1995), their subunit interactions are distinct from those observed for the She2p dimer.

Amino acid sequence identities within the fumarase/aspartase homologous superfamily tend to be high (Woods et al., 1986) (e.g., *E. coli* and human fumarase C are 59% identical), but none of the proteins enumerated above are more than 12% identical to She2p. Sequence identities between She2p and fumarase/aspartase superfamily homologs from *S. cerevisiae* do not exceed 11%. A signature sequence motif found within the central domain of fumarase/aspartase superfamily members, which consists of a highly conserved, functionally important region (Estevez et al., 2002), is also lacking in She2p. Unlike She2p, proteins of the fumarase/aspartase superfamily consist of three domains, and their central domain lacks the small protruding helix of She2p. To the best of our knowledge, nucleic acid binding activity has not been reported for any member of the fumarase/aspartase superfamily.

In summary, similarities between She2p and the central domains of fumarase/aspartase superfamily mem-

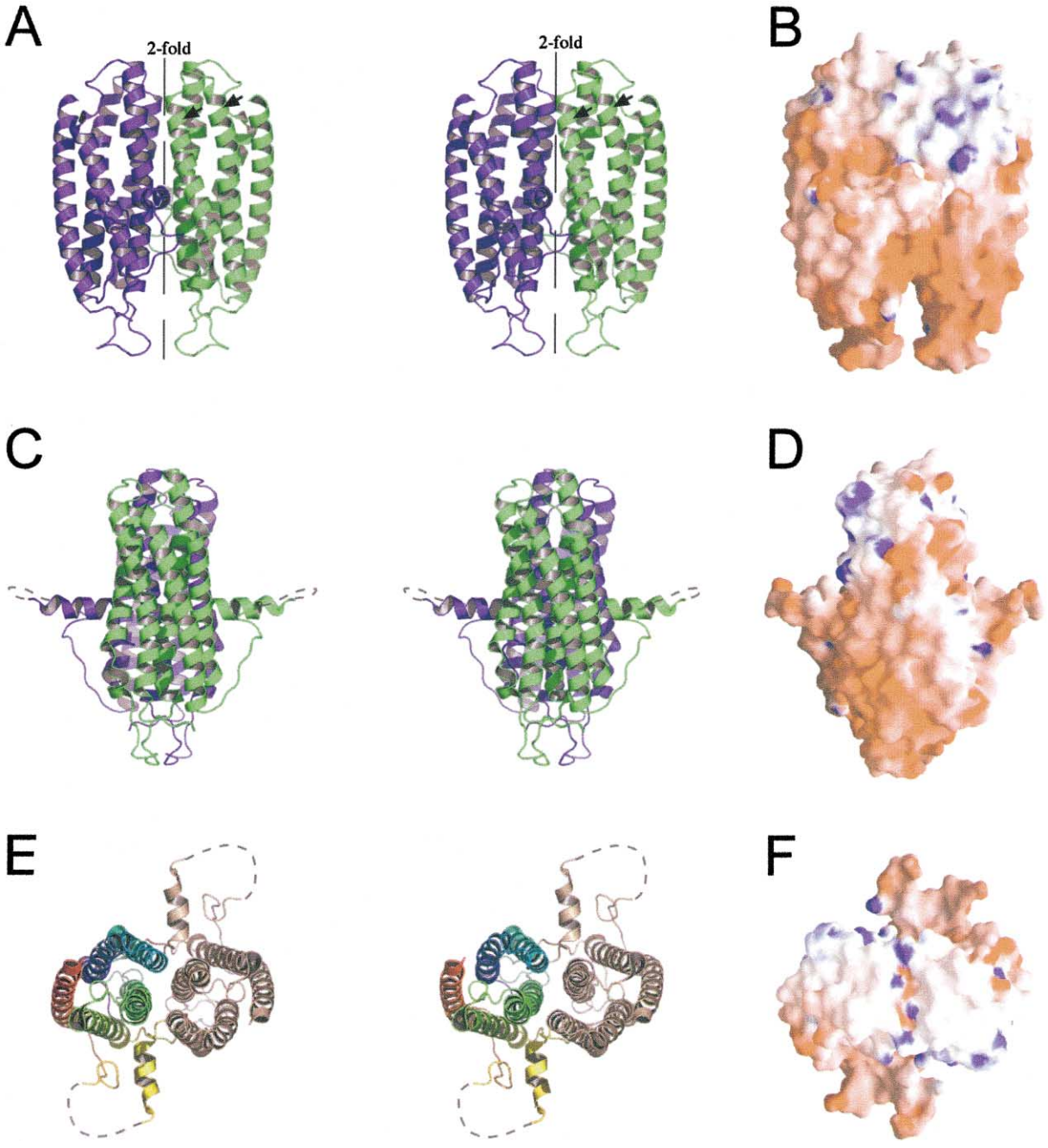

Figure 1. Structure of the She2p Homodimer

(A) Stereoview of the She2p homodimer with each monomer in blue or green (PyMOL, DeLano Scientific, CA). The second, less complete monomer was substituted with a superimposed first monomer to provide a fuller depiction of the She2p homodimer. Vertical line labeled with "2-fold" indicates the axis of 2-fold noncrystallographic symmetry relating the halves of the homodimer. Arrows on the green subunit denote the two α helices of the basic helical hairpin, containing residues required for RNA binding (not indicated for the blue subunit; for details, see text).

(B) GRASP (Nicholls et al., 1993) surface representation of the chemical properties of the solvent-accessible surface of She2p, using a water probe radius of 1.4 Å. The surface electrostatic potential is color coded red and blue, representing electrostatic potentials between < -14 to $> +14$ k_BT, where k_B is the Boltzmann constant and T is the temperature. Orientation is identical to (A).

(C) Stereoview of (A) rotated 90° around the vertical axis. Dotted lines represent an eight amino acid gap in the final refinement model.

(D) GRASP surface representation of (B) rotated 90° around the vertical axis.

(E) Stereoview of (A) rotated 90° around the horizontal axis, with the top of She2p turned toward the reader. Rainbow coloration of one monomer follows the polypeptide chain, with the N terminus in blue and the C terminus in red. The second monomer is colored brown.

(F) GRASP surface representation of (B) rotated 90° around the horizontal axis, with the hydrophobic upper surface of She2p facing the reader.

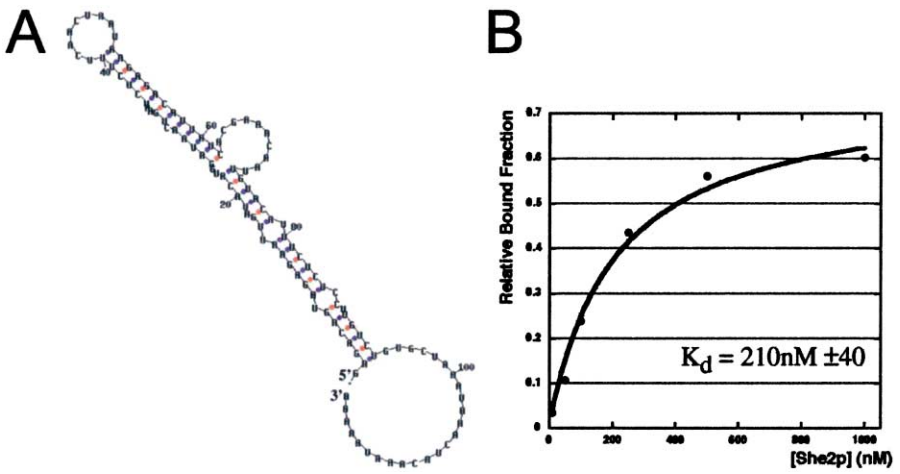

Figure 2. Structural Prediction and Analysis of She2p RNA Binding

(A) Secondary structure prediction (Mfold; Zucker, 1998) for the *ASH1* mRNA E3 zip code element as previously described by Chartrand et al. (1999).

(B) Filter binding results with She2p (wild-type) and the E3 zip code element of *ASH1* mRNA (K_d = 210 nM ± 40). Since C-terminal residues of She2p are required for efficient RNA binding (data not shown), no binding studies were performed with the N- and C-terminally truncated version of She2p used for crystallization.

bers are strictly limited to the overall structural arrangement of their respective five α helix core, with no apparent evolutionary conservation or functional homology. We conclude, therefore, that She2P represents a novel protein fold of distinct evolutionary origin that is not currently represented in the PDB.

She2p Binds ASH1 RNA with nM Affinity

The core function of She2p is to bind *ASH1* mRNA and initiate assembly of the *ASH1* mRNP (Böhl et al., 2000; Chartrand et al., 1999; Gonzalez et al., 1999; Long et al., 2000). To date, no quantitative information on She2p RNA binding is available, raising the question as to whether or not RNA binding by She2p suffices to recruit *ASH1* mRNA into mRNP complexes in vivo. We determined the affinity of wild-type She2p for the single zip code element E3 of *ASH1* mRNA using filter binding assays (see Figure 2A for the results of RNA secondary structure prediction). She2p binds its target RNA with an equilibrium dissociation constant (K_d) of 210 nM (±40; Figure 2B).

A calculation of She2p abundance in vivo (4070 molecules per cell, Ghaemmaghami et al. [2003]; cell volume, 30 μm^3, Tyson et al. [1979]) suggests that She2p is present at a cellular concentration of about 230 nM. As She2p is localized in yeast cells, the effective concentration is almost certainly higher. Although this calculation is unlikely to provide an accurate estimate of She2p concentration in cells, it suffices to support our conclusion that She2p is present at concentrations at or above its RNA binding K_d. She2p should, therefore, be able to recruit target mRNA into mRNP complexes in vivo. It is remarkable that She3p association with the She2p:*ASH1* mRNA complex further increases the affinity of the growing complex for *ASH1* mRNA (Böhl et al., 2000). This effect would serve to ensure recruitment of *ASH1* mRNA into a productive mRNP complex at She2p concentrations less than the K_d and to enhance the efficiency of *ASH1* mRNA translocation in mating-type switching repression.

She2p Binds RNA via a Positively Charged Surface Feature

Analysis of the solvent-accessible molecular surface (Nicholls et al., 1991) of She2p revealed an overall negative electrostatic potential, with the exception of a distinct surface area with positive electrostatic potential (Figures 1B, 1D, and 1F). We mapped all previously identified RNA binding residues (Gonsalvez et al., 2003) to the surface feature with positive electrostatic potential (Figure 3A, marked with asterisk; Figure 3B). In addition, we produced and analyzed various mutant forms of She2p binding to *ASH1* RNA. Only those amino acids located within the surface feature with positive electrostatic potential were required for RNA binding (Figures 3A and 3B).

Together, these results define a basic helical hairpin RNA binding motif consisting of two antiparallel α helices separated by a loop (Figure 3C). Within this local tertiary structural feature, we find the following sequence motif: N-x(6)-[KR]-[KR]-loop-x(7)-R-x(4)-K-x(2)-K-x(2)-R, where "x(n)" indicates "n" residues, "[KR]" indicates either a lysine or an arginine, and "loop" marks the position where two α helices are connected by a loop. In Figure 1A, this region of the polypeptide chain is located on the right (green) monomer in the upper half of the two foremost α helices (marked with arrows) and for the left (blue) monomer in the corresponding position on the rear surface of the homodimer (not marked).

Within the same dimer subunit (A) and adjacent to the positively charged RNA binding motif, we sought additional residues necessary for nucleic acid binding. None of the following A subunit mutations (His33→Ala, Arg49→Ala, Asp67→Ala, Thr235→Tyr) affected RNA binding. Mutation of the following residues from the B subunit of the homodimer (Gln119→Ala, Lys123→Ala, Lys179→Ala), which are positioned close to the A monomer RNA binding motif, does not affect RNA binding in vitro (Figures 3A and 3B). We conclude, therefore, that the basic helical hairpin serves as the primary anchor for *ASH1* mRNA to each half of the homodimer.

A

RNA-binding mutants

Protein	RNA-binding	Protein	RNA-binding
Wildtype	K_d = 210nM ± 40nM	R52K*	-
		K57A	+/-
H33A	wt	K60A	-
N36S*	-	R63A*	Insoluble
R43A*	+/-	R63K*	-
R43K*	wt	R63D	-
R44A*	+/-	D67A	wt
R44K*	wt	Q119A	wt
R49A*	wt	K123A	wt
R49K*	wt	K179A	wt
R52A*	-	T235Y	wt

* Gonsalvez et al., 2003: these She2-mutants were testet for RNA-binding by three-hybrid assay.

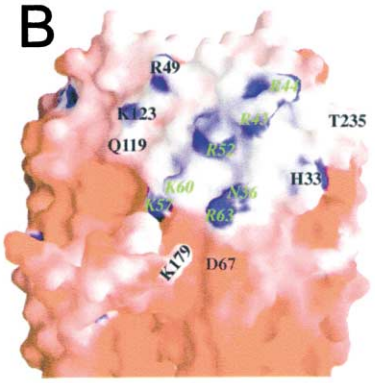

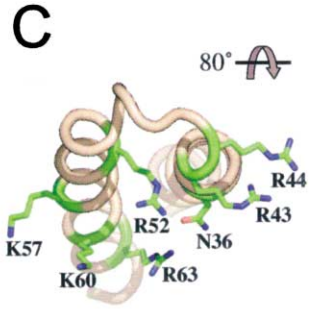

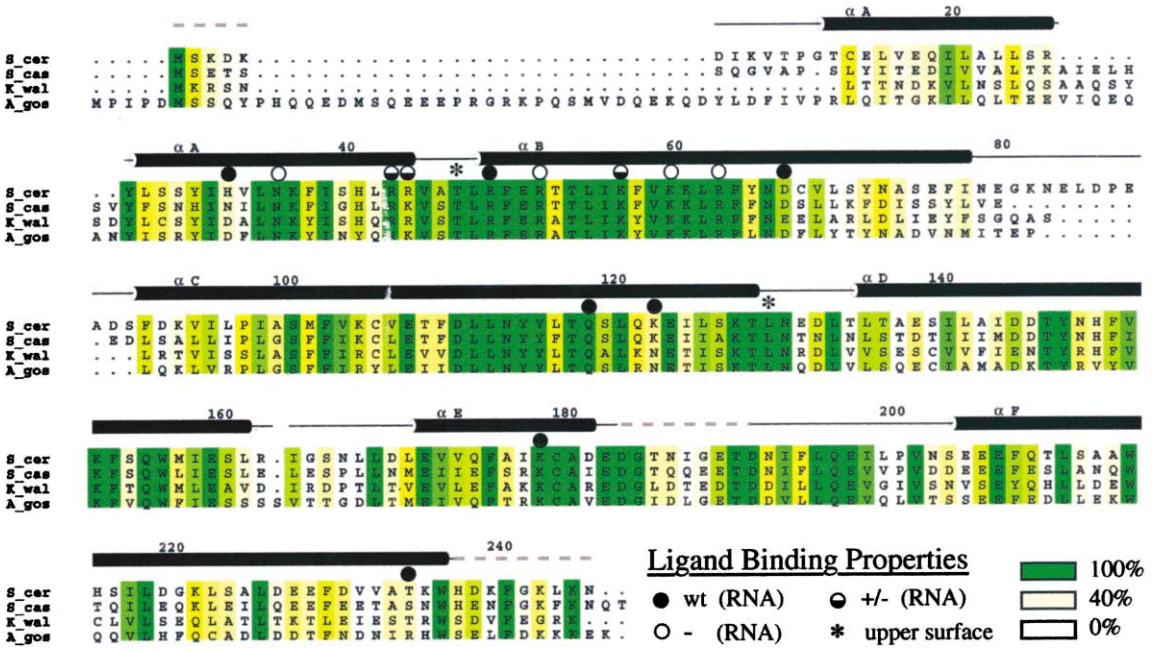

Figure 3. She2p Dimer Binds RNA via a Conserved, Basic Helical Hairpin

(A) Table summarizing RNA binding properties of mutant forms of She2p from filter binding experiments (this study) and yeast three-hybrid studies (asterisk; Gonsalvez et al., 2003): "wt," "+/−," and "–" denote wild-type, reduced, and not-detectable RNA binding affinity, respectively. The mutant form She2p Arg63→Ala was previously described as being defective in RNA binding (Gonsalvez et al., 2003). In our hands, She2p Arg63→Ala was insoluble. Instead, we generated She2p Arg63→Asp and determined that this soluble mutant form of She2p does not bind RNA.

(B) Enlarged view of GRASP surface representation shown in Figure 1B, rotated 10° around the horizontal axis and 15° counterclockwise around the vertical axis. Labels shown in green with italics overlay residues required for RNA binding. Black labels overlay the sites of mutations that do not affect RNA binding (see Figure 3A).

(C) Schematic of the basic helical hairpin of She2p viewed from above and slightly rotated from the orientation shown in Figure 1E. The polypeptide backbone for residues 25–68 is colored brown, with the exception of green color-coded basic residues for which the side chains are also depicted.

(D) Sequence alignment of She2p. Secondary structural elements were obtained from the X-ray structure. Dashes denote residues that were either disordered or excluded from the recombinant form of She2p used for crystallization. Full, half-filled, and empty circles denote sites of mutations resulting in wild-type, reduced, and negligible RNA binding, respectively (see also Figures 3A and 3B). "*" denotes amino acids that are required for *ASH1* mRNA binding (Figures 5C and 5E), interaction with She3p (Leu130; Gonsalvez et al., 2003), and translocation of *ASH1* RNP in vivo (Leu130; Gonsalvez et al., 2003), which are located outside the RNA binding surface feature with positive electrostatic potential. Sequence similarity is encoded by a yellow-to-green color gradient, representing 40%–100% identity (BLOSUM62).

Sequence Conservation in She2p Reveals Regions of Functional Importance

We used the RNA binding sequence motif found within the basic helical hairpin to search for similar motifs in proteins of 18 other yeasts (http://www.yeastgenome.org; partially and completely available genomes). Pattern matching detected nine independent amino acid sequences, all of which proved to be related to *S. cerevisiae* She2p (e value cutoff for full-length She2p = 1×10^{-30}). Among these matches were She2p orthologs found in two distantly related yeasts, *Kluyveromyces waltii* (Kellis et al., 2004) and *Ashbya gossypii* (Dietrich et al., 2004), which also encode homologs of all known core proteins comprising the *ASH1* mRNP complex.

We used ClustalX (Thompson et al., 1997) to perform an amino acid sequence alignment of She2p from *S. cerevisiae* and its orthologs from *S. castellii*, *K. waltii*, and *A. gossypii* (Figure 3D). The resulting sequence

alignment reveals pairwise sequence identities to *S. cerevisiae* She2p of 51.4% (*S. castellii*), 42.6% (*K. waltii*), and 40.2% (*A. gossypii*). The remarkable level of sequence identity and the pattern of amino acid differences among these yeast strains allow us to conclude that all known She2p proteins share the same three-dimensional structure (Sander and Schneider, 1991). Comparative protein structure modeling (Pieper et al., 2004) with our structure of She2p from *S. cerevisiae* was used by Sali and coworkers to produce reasonably accurate structural models of all known She2p homologs. The resulting structural models are available to academic users via http://salilab.org/modeller/modeller.html.

Of the seven She2p RNA binding residues identified in this work and Gonsalvez et al. (2003) (Figures 3A and 3B), six are identical in all species, and one residue demonstrates a conservative exchange in *S. castellii* and *A. gossypii* (Arg44→Lys). This conservative exchange has been shown in *S. cerevisiae* to functionally substitute for arginine (Figure 3A) (Gonsalvez et al., 2003). Near-total conservation of the She2p RNA binding basic helical hairpin motif supports our contention that residues of functional importance are highly conserved among She2p family members. As more genomic sequences of yeasts become available, additional conserved surface features may become apparent, allowing us to discern other functionally important surface regions.

We attempted to extend our analysis of candidate proteins bearing a *S. cerevisiae* She2p-like basic helical hairpin motif (Figures 3A–3C) by searching a protein sequence database that includes proteins from non-yeast species (Swissprot; http://motif.genome.jp; variable sequence length for the loop). The search yielded seven candidate proteins (50S ribosomal protein L13P, *Sulfolobus solfataricus*; transcription factor ICE1, *Arabidopsis thaliana*; RNA helicase Senataxin, *Homo sapiens*; viral core protein VP6, bluetongue virus; CbbX protein homolog, *Guillardia theta*; mannitol-1-phosphate-5-dehydrogenase, *Mycoplasma mycoides*; and transient receptor potential channel, *Caenorhabditis elegans*), of which four are thought to bind nucleic acids. Two of these known nucleic acid binding proteins, the 50S ribosomal protein L13P and the transcription factor ICE1, are members of known structural classes that do not resemble She2p and do not in fact contain basic helical hairpins. No structural information is available for any of the five remaining candidate proteins. Secondary structure predictions were used to look for evidence of putative helical regions within the appropriate segments matching the basic helical hairpin sequence motif from She2p. At best, the results of these analyses were ambiguous. Given our current, somewhat limited, knowledge of the universe of three-dimensional protein structures, it appears that the basic helical hairpin motif occurs only within She2p proteins and their homologs in yeasts.

Dimerization of She2p Is Required for RNA binding

Since She2p forms a stable dimer in solution, we sought to establish whether or not She2p dimerization is required for RNA binding. Guided by our structure of She2p, we selected two single amino acid substitutions (Cys68→Tyr and Ser120→Tyr, respectively) intended to produce unfavorable steric clashes at the dimer interface and thereby prevent She2p subunit joining. Analyses of the two mutant proteins by size exclusion chromatography indicated a significantly lower molecular weight for both mutant proteins as compared to wild-type She2p (data not shown). Measurement of RNA binding affinities revealed that both mutant proteins were unable to bind *ASH1* RNA efficiently (Figure 4A). (Circular dichroism [CD] spectroscopy documented identical secondary structural composition for mutant and wild-type She2p [data not shown], making it extremely unlikely that loss of RNA binding activity is an artifact of mutant She2p unfolding or misfolding.) Our results, therefore, document that She2p dimerization is required for *ASH1* mRNA binding.

She2p Function In Vivo

In yeast cells, She2p binding to *ASH1* mRNA is required for assembly of *ASH1* mRNP and translocation to the daughter cell tip. Mutant forms of She2p that do not bind *ASH1* RNA in vitro should not, therefore, translocate *ASH1* mRNA to the bud tip.

In order to validate our in vitro findings, a *SHE2* deletion strain was transformed with plasmids expressing either wild-type or various *she2* mutant alleles under control of the *SHE2* promoter. The *ASH1* mRNA localization properties of different *she2* alleles were tested with fluorescent in situ hybridization using Cy3-labeled probes against *ASH1* mRNA. In a strain expressing wild-type She2p, *ASH1* mRNA is localized to the bud tip of the daughter cell, whereas, in a *she2* deletion yeast strain, *ASH1* mRNA is found distributed throughout mother and daughter cell (Figures 4B and 4G and Figures 4C and 4H, respectively). In vitro, the mutant form She2p Lys60→Ala is not able to bind RNA (Figure 3A). Confirming the requirement of She2p RNA binding for in vivo function, She2p Lys60→Ala does not localize *ASH1* mRNA in vivo (Figures 4D and 4I). The mutation Asp67→Ala, which lies outside of the She2p RNA binding domain and supports RNA binding in vitro, yields a mutant form of She2p that is competent for *ASH1* mRNA localization to the bud tip of the daughter cell (Figures 4E and 4J). Finally, one of the two mutations (Ser120→Tyr) that interfere with dimerization and RNA binding (Figure 4A) yields a form of She2p that also cannot localize *ASH1* mRNA in vivo (Figures 4F and 4K).

In summary, the yeast translocation studies support our previous findings by showing a direct correlation between in vitro She2p-RNA binding efficiency and *ASH1* mRNA translocation. Our in vivo yeast studies also establish the requirement of She2p-homodimer formation for translocation, which itself is necessary for RNA binding activity in vitro.

A Conserved, Uncharged Surface Feature Is Required for She2p Function

To identify additional conserved surface regions of functional importance, we analyzed a surface representation of the She2p-sequence alignment (Figures 3D and 5A–5D). In addition to the previously defined RNA binding surface feature (Figures 5A–5C; enclosed with dotted

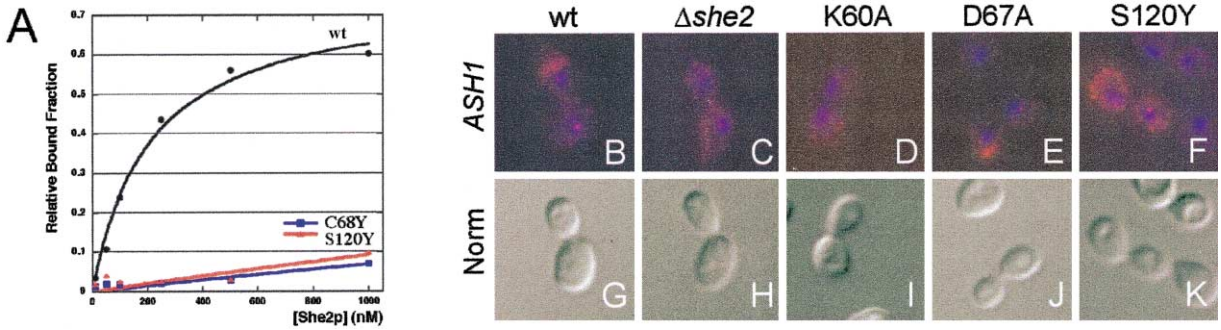

Figure 4. Defective She2p Function Interferes with RNA Binding and ASH1 mRNA Localization at the Bud of the Daughter Cell

(A) Filter binding experiments with dimerization-defective forms of She2p and the E3 zip code element of *ASH1* mRNA. Both dimer mutant forms of She2p fail to bind RNA efficiently.

(B–F) In situ hybridization with Cy3-labeled oligonucleotides against *ASH1* mRNA after transformation of *SHE2* deletion strain with constructs expressing either the wild-type *SHE2* allele (B), plasmid without *SHE2* (C), or various mutant *she2* alleles (D–F). *ASH1* mRNA is depicted in red and DAPI nuclear staining in blue. Images depict representative cell staining.

(G–K) Images show identical views to those depicted in (B)–(F) acquired with Normarski optics.

lines), the small protuberant helix and its connection to the five α helix bundle is conserved. Surface features at the side (Figure 5B) and the bottom of She2p (Figure 5D) show little and no conservation, respectively. The upper surface region of She2p, which is largely uncharged (Figure 1F), contains hydrophobic amino acids, and consists of surface features from both dimer subunits, shows a high degree of sequence conservation (Figure 5C).

In order to characterize the functional relevance of the conserved upper surface region of the She2p dimer, we generated two independent amino acid exchanges within this area (Thr47→Tyr and Leu130→Tyr, respectively; Figure 5C). Filter binding experiments with recombinant She2p Thr47→Tyr and She2p Leu130→Tyr showed reduced RNA binding activities for both mutant proteins (Figure 5E), demonstrating a functional requirement for the upper surface feature of She2p. Comparative analysis of wild-type She2p and She2p Leu130→Tyr by CD spectroscopy documented no significant differences in secondary structural composition (data not shown).

It is remarkable that Golsalvez et al. (2003) isolated a yeast strain bearing a Leu130→Ser mutation in She2p that does not translocate *ASH1* mRNA in yeast (see Supplemental Material, Table S1, in Gonsalvez et al. [2003]). In addition, they showed that recombinant Leu130→Ser mutant She2p is unable to bind She3p. In contrast, other RNA binding-defective mutants described by Gonsalvez et al. (2003) (Figure 3A, marked with asterisk) retain She3p binding. Our findings with the Thr47→Tyr and Leu130→Tyr mutant forms of She2p, together with the reported loss of translocation in She2p Leu130→Ser mutants (Gonsalvez et al., 2003), indicate that the upper, uncharged surface region of She2p is required for *ASH1* mRNA binding and translocation in vivo.

One She2p Dimer Binds to One ASH1 mRNA Zip Code Element

She2p dimer formation is required for *ASH1* mRNA zip code element binding, suggesting two possible modes of She2p-zip code element interaction. The first possibility involves the binding of one RNA zip code element to each basic helical hairpin containing side of the dimer, resulting in a ratio of dimer to zip code element of 1:2 (Figure 5F). The second possible mode requires that one zip code element binds to one dimer, resulting in a dimer to zip code element ratio of 1:1 (Figure 5G).

In order to distinguish between these two possibilities, we performed filter binding experiments with near stoichiometric ratios of She2p and *ASH1* mRNA E3 zip code elements. The observed ratio of She2p dimer to zip code element at saturation is 1:1.28 (Figure 5H), indicating that one She2p dimer binds to one RNA zip code element.

Discussion

Our studies demonstrate that She2p represents an RNA binding protein of novel three-dimensional structure. She2p forms a stable dimer in solution, and dimer formation is required for *ASH1* mRNA binding in vitro and mRNA translocation in yeast. We showed that She2p binds *ASH1* mRNA in vitro with sufficient affinity to support effective recruitment into functional mRNP complexes in vivo and identified a helical hairpin RNA binding motif, which is displayed on a conserved surface feature with positive electrostatic potential. Moreover, our results, together with structure-based interpretation of previously published findings, demonstrate that a conserved, uncharged surface feature on top of She2p is required for efficient RNA binding, recruitment of factors into the She2p:RNA complex, and translocation in yeast.

The E3 zip code element, which was used in filter binding experiments, is thought to contain an extended stem-loop secondary structure (Figure 2A). Binding studies with mutated E3 zip code elements showed that the predicted RNA loop region at the tip of the putative double-stranded stem is dispensable (Chartrand et al., 1999). Mutations altering the secondary structure of the putative double-stranded stem result in a loss of She2p binding, whereas She2p binding is not impaired when bases on both complementary strands are exchanged, without destabilizing the predicted secondary structure

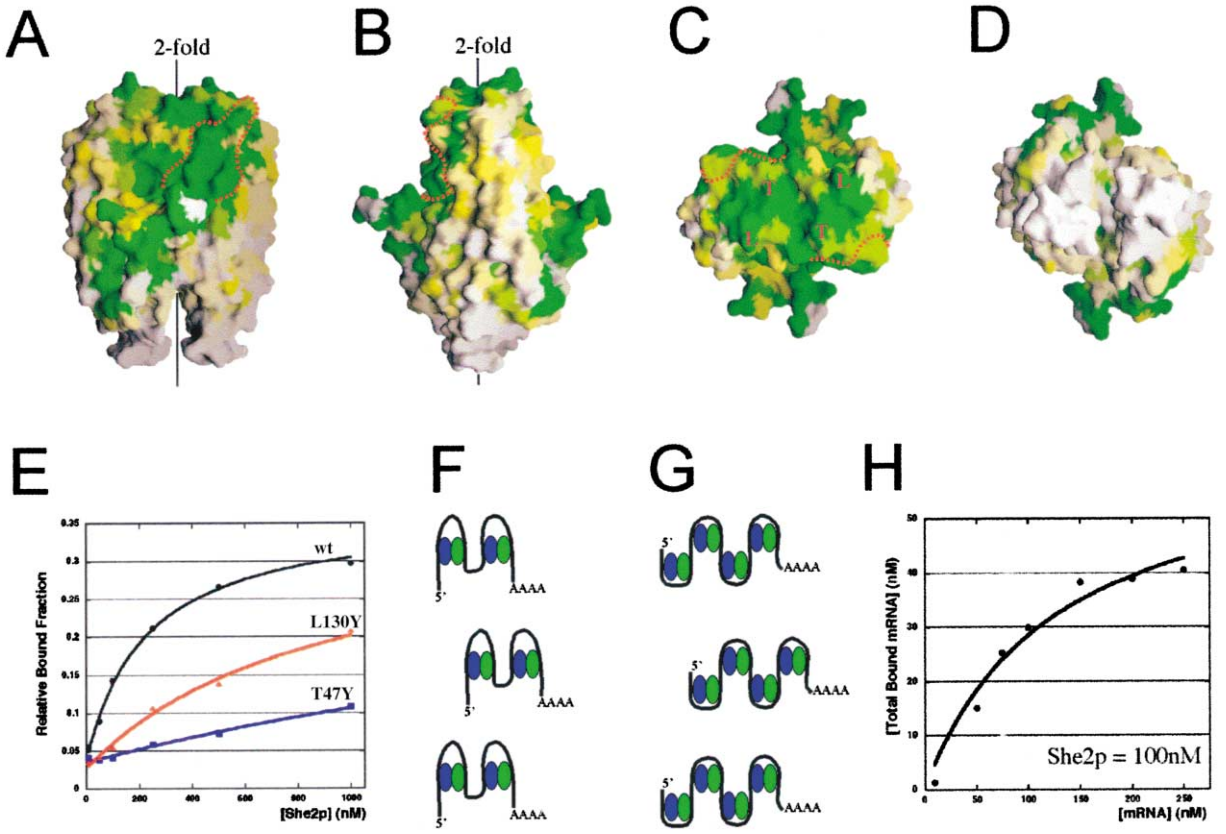

Figure 5. Sequence Conservation Identifies Functional Surface Features

(A) GRASP surface representation of sequence conservation as shown in Figure 3D with identical orientation as in Figure 1B. The dotted line encloses surface residues responsible for RNA binding.

(B) GRASP surface representation of (A) with orientation as in Figure 1D.

(C) GRASP surface representation of (A) with orientation as in Figure 1F. "T" and "L" denote Thr47 and Leu130 on both dimer subunits (see Figure 5E).

(D) GRASP surface representation of (A), with orientation of (C) rotated 180° around the horizontal axis (bottom view instead of view on upper surface of She2p).

(E) Filter binding experiments with mutant forms of She2p that contain amino acid exchanges in its upper, uncharged surface region (see also [C]), and the E3 zip code element of *ASH1* mRNA. She2p Thr47→Tyr and She2p Leu130→Tyr show strong and modest reduction in affinity for *ASH1* mRNA, respectively.

(F and G) Schematics depicting potential modes of She2p dimer binding to the four independent zip code elements of *ASH1* mRNA, as discussed in the main body of the paper.

(H) Filter binding experiments with 100 nM wild-type She2p and increasing, near-stoichiometric amounts of E3 zip code element of *ASH1* mRNA (up to 2.5-fold excess). The projected maximum bound RNA concentration of 64 nM indicates a ratio of She2p dimer to RNA zip code element of 1:1.28, suggesting that one She2p dimer binds one zip code element (see Figure 5G).

(Böhl et al., 2000; Chartrand et al., 1999, 2002; Gonzalez et al., 1999). These results together with the findings of our structural and mechanistic studies suggest that She2p binds *ASH1* mRNA by recognizing RNA secondary structure via interactions with its residues displayed by the basic helical hairpin (Figure 3C) and on the conserved hydrophobic feature on the upper surface of the homodimer depicted in Figure 1F.

Since She2p homodimer has two RNA binding motifs, it is intriguing to speculate that one She2p homodimer binds two independent zip code elements. Two She2p homodimers would suffice for efficient binding to all four known zip code elements of one *ASH1* transcript (Figure 5F).

In contrast to this model, our filter binding experiments under near-stoichiometric concentrations indicate that one zip code element binds around one She2p homodimer, requiring four She2p homodimers to bind all four zip code elements of *ASH1* mRNA (Figures 5G and 5H). In addition to residues from the RNA binding surface feature with positive electrostatic potential, mutations on the upper, uncharged surface feature of She2p impair RNA binding. These findings suggest that one *ASH1* mRNA zip code element arches over the upper, uncharged She2p surface region and binds simultaneously to the basic helical hairpins of both monomers. To date, the smallest identified *ASH1* zip code element has a length of 77 bases (*ASH1* U element) and is believed to form a double-stranded stem-loop structure (Böhl et al., 2000; Gonzalez et al., 1999). Manual alignment of modeled dsRNA to the RNA binding surface features of She2p dimer indicates that a 77 base dsRNA would be large enough to arch over the upper surface region of She2p and interact with both positively

charged RNA binding surface features simultaneously (data not shown).

This mode of RNA binding, in which a She2p dimer uses both subunits to bind one zip code element (Figure 5G), also explains the requirement of She2p dimerization for RNA binding. Moreover, it is consistent with the results of recent biophysical studies of yeast myosins type II and V, which showed that ca. four motor proteins are required to move cargo continuously (Reck-Peterson et al., 2001). Four myosin V motors are also thought to be required for processivity of *ASH1* mRNA transport (Chartrand et al., 2002).

ASH1 mRNP complex assembly requires She3p joining the She2p:RNA complex. We speculate that She3p interacts with a heterologous surface region, consisting of She2p and dsRNA. The requirement for a heterologous surface region for She3p binding could explain why She3p interacts efficiently with She2p:RNA and not with She2p alone (Long et al., 2000) and why She3p stabilizes She2p-RNA interaction (Böhl et al., 2000). Such an mRNA-dependent assembly mechanism of the *ASH1* mRNP may ensure that the translocation complex does not engage in a futile transportation of core factors into the bud cell in the absence of cargo mRNA.

A surface representation of sequence conservation (Figures 5A–5D) demonstrated that the protuberant helix and the upper, uncharged surface region of She2p are highly conserved. Given correlations between sequence conservation and functional importance (Figure 3D), we speculate that one or both of these conserved regions participates in formation of a (heterologous) surface for She3p binding. The uncharged region of She2p with its hydrophobic amino acids represents an unusual feature on the surface of an otherwise charged protein (Figures 1B, 1D, and 1F). Interactions between proteins and nucleic acids are generally mediated by charged amino acids (Nadassy et al., 1999; Nagai, 1996), whereas protein-protein interactions can involve both uncharged, hydrophobic surface areas and charged amino acids (Conte et al., 1999; Dasgupta et al., 1997). It is, therefore, possible that, in addition to its requirement for efficient *ASH1* mRNA binding, the uncharged surface region of She2p mediates interactions with She3p. A previously published report that She2p bearing a mutation in the uncharged surface region (Leu130→Ser) fails to interact with She3p (see Supplemental Material, Table S1, in Gonsalvez et al. [2003]) is consistent with this speculation. Future structural and functional studies will be necessary to understand precisely how She2p binds *ASH1* mRNA and how interactions with She3p influence the formation of a functional localization complex.

Experimental Procedures

Protein Preparation, Quality Assurance, and Crystallization

cDNAs encoding various forms of She2-P (full-length, 246 residues) from *S. cerevisiae* were expressed in *E. coli* Bl21-DE3* as glutathione S-transferase fusion proteins in the vector pGEX6p-1. Each expressed protein was purified to homogeneity via glutathione-Sepharose chromatography, followed by subtractive glutathione-Sepharose and anion exchange chromatographies and a final size exclusion chromatography step. Protein purity and quality were assessed by gel electrophoresis, size exclusion chromatography, MALDI-MS (Cohen and Chait, 2001), and dynamic light scattering (Ferré-D'Amaré and Burley, 1997). Purified proteins contained the wild-type She2p-peptide sequence plus a five amino acid N-terminal linker region, unless stated otherwise.

Initial, poor-quality crystals were obtained by hanging drop vapor diffusion against 0.1 M Na-HEPES (pH 7.5), 1.5 M $LiSO_4$, and 2 mM TCEP at 20°C. Analyses of She2p, both from solution and from these poor-quality crystals, revealed evidence of unwanted intermolecular disulfide bond formation. Alkylation of She2-P with N-ethyl-maleimide or iodoacetamide under anaerobic conditions combined with electrospray ionization mass spectrometry (ESI-MS) (Vinkemeier et al., 1996) suggested that all four cysteines in She2p are solvent exposed and capable of forming intermolecular disulfide bonds. Cys14, Cys68, Cys106, and Cys180 were simultaneously mutated to serines. Based on results from limited proteolysis combined with MALDI-MS and ESI-MS (data not shown; Cohen and Chait, 2001), we generated multiple N- and C-terminal truncations of She2p and tested a total of 20 truncated forms of She2p in crystallization trials.

Diffraction-quality crystals of She2p (residues 6–239, with Cys14, Cys68, Cys106, and Cys180 mutated to serines) were obtained at a protein concentration of 2–2.5 mg/ml via hanging drop vapor diffusion against 50–100 mM Tris (pH 8.5), 160–200 mM $LiSO_4$, 20%–25% PEG 4000 (w/v), and 2.4 mM β-octyl-glucoside at 20°C. Diamond-shaped crystals appeared after 2–4 days, which grew to a typical size of $0.05 \times 0.1 \times 0.1$ mm^3. Crystal cryoprotection was achieved by adding ethylene glycol to a final concentration of 30% (v/v). No crystals were obtained from Se-Met-substituted She2p. Experimental phases were measured from crystals soaked in crystallization solution with various heavy metals present at concentrations ranging from 1 to 100 mM for 1–4 days.

Data Collection, Structure Determination, and Refinement

All diffraction data were collected at the SGX-CAT insertion device beamline at the Advanced Photon Source (Argonne National Laboratory) under standard cryogenic conditions and processed and scaled using DENZO and SCALEPACK (Otwinowski and Minor, 1997). A total of 24 datasets was collected (Table 1; for all crystals examined in the different experiments, space group C2; unit cell a = 97.2 Å, b = 103.7 Å, c = 57.7 Å, β = 110.5°, ± <1%; two She2 molecules/asymmetric unit). Ta_6Br_{12} cluster binding sites were located using direct methods (SnB, Weeks and Miller [1999]), and four independent $IrCl_3$ sites were obtained by Fourier difference syntheses from initial Ta_6Br_{12}-derived phases. Definitive experimental phases were obtained via multiple isomorphous replacement using CCP4/MLPHARE (Collaborative Computational Project, 1994) (three Ta_6Br_{12} sites [one data set]; four independent $IrCl_3$ sites [three datasets]) for two independent datasets at 1.95 Å (Table 1, Native[a]) and 2.35 Å (Table 1, Native[b]) resolution, respectively. After density modification (CCP4/DM), both native data sets yielded electron density maps that showed interpretable density features in complementary regions of each map. After merging the electron density maps, ten large α-helical features were immediately recognizable within the asymmetric unit. The merged electron density map revealed the noncrystallographic symmetry (NCS) operator relating dimer subunits. After NCS averaging and further density modification, the secondary structural features for most of the pentacle core of the She2p homodimer were readily apparent. Automated electron density map interpretation with MAID (Levitt, 2001) yielded atomic models encompassing an average of 103 residues per molecule (206 residues per asymmetric unit). Iterative rounds of refinement and model building gave the current refinement model, with the working R_{factor} = 19.1% and an R_{free} value of 24.1% (residues 6–183 and 192–237 for the first molecule in the asymmetric unit and residues 13–76, 92–177, and 204–237 for the second molecule in the asymmetric unit, plus 302 isolated density features modeled as water molecules). PROCHECK (Laskowski et al., 1993) revealed 93% of (ϕ, ψ) combinations in the most favorable region of the Ramachandran diagram and an overall G factor of −0.1, which is significantly better than average for structures obtained at ~2 Å resolution.

Analytical Ultracentrifugation

Sedimentation equilibrium measurements were made to determine the oligomerization state of She2p in solution. Data were collected at the Keck Biophysics Facility at Northwestern University (Evanston, IL) with an XL-A analytical ultracentrifuge (Beckmann, Fullerton,

Table 1. Data Statistics

Data Sets	Native[a]	Native[b]	Ta_6Br_{12}	$IrCl_3$ #1	$IrCl_3$ #2	$IrCl_3$ # 3
Space group	C2	C2	C2	C2	C2	C2
Resolution (Å)	25–1.95	25–2.35	25–2.7	25–3.15	25–3.35	25–2.5
Reflections, overall/unique	120,406/37,528	24,265/43,047	267,556/14,794	367,276/9262	162,289/7582	542,714/35,187
Completeness (%), overall/outer shell	98.0/97.2	99.9/99.9	99.9/99.9	99.9/99.9	99.8/99.9	99.9/99.9
$<I/\sigma(I)>$, overall/outer shell	11.1/2.7	12.7/2.9	15.5/6.7	14.3/3.8	14.2/3.5	11.6/2.7
$R_{sym}(I)$ (%), overall/outer shell	8.6/48.6	8.4/47.6	9.9/29.7	10.8/47.4	8.7/39.4	9.9/48.1
Wavelength (Å)	1.072	1.023	0.920	0.920	0.920	0.920
Overall figure of merit	0.289	0.296	–	–	–	–
Phasing power (iso) (Native[a])	–	–	1.02	0.79	0.89	0.71
Phasing Power (iso) (Native[b])	–	–	0.90	1.14	1.23	0.65

[a] Crystal soaked in 1mM K_2PtI_6.

[b] Crystal soaked in 1 mM $(NH_4)_2WS_4$. R_{sym} (I) = $\Sigma|I - <I>|/\Sigma I$, where I = observed intensity and $<I>$ = average intensity obtained from multiple observations of symmetry related reflections. Phasing power = rmsd ($|F_H|/E$), with $|F_H|$ = heavy atom structure factor amplitude, and E = residual lack of closure. Data set "Native[a]" was used for refinement and iterative model building.

CA) and processed using the software ULTRASCAN 6.2 (B. Demeler, UTHSC San Antonio, TX). She2p full-length (Cys14→Ser, Cys68→Ser, Cys106→Ser, and Cys180→Ser) in 150 mM KCl and 10 mM Tris/HCl (pH 7.5) was examined at concentrations of 7.9 μM; 15.9 μM; 23.8 μM; and 31.7 μM (corresponding to optical densities at 280 nm, 0.2, 0.4, 0.6, and 0.8) at 17,000; 25,500; 34,000; 42,500; and 50,000 rpm. The major oligomerization state of She2p was dimeric, with no evidence of monomer formation. Problems with time-dependent sample aggregation precluded further quantitative experiments and analyses.

Circular Dichroism Spectroscopy

Data were collected and processed with a Circular Dichroism Spectrometer Model 215 (Aviv Instruments). She2 full-length (wild-type, Cys68→Tyr, Ser120→Tyr, or Leu130→Tyr) in 100 mM KCl, 5 mM Tris/HCl (pH 7.5), and 0.1 mM TCEP were examined at a concentration of 7.9 μM (optical density at 280 nm, 0.2) between 192 and 250 nM (step size, 1 nM).

Yeast Expression of SHE2 Mutants

A *SHE2* expression cassette for full-length She2p (wild-type and mutants described in Figures 4B–4K) was constructed by ligating two PCR products into XhoI endonuclease sites. The PCR products were amplified from genomic DNA spanning 500 bp upstream and downstream of the *SHE2* open reading frame and adding an EcoRI restriction site after the start codon and an HA epitope to the 3′ end of the coding sequence, respectively. This expression cassette was ligated at KpnI and XmaI endonuclease sites into pRS414, creating the pRS414 *SHE2* HA cassette. Wild-type and mutant *SHE2* were amplified by PCR and ligated at EcoRI and XhoI endonuclease sites into the pRS414 SHE2 HA cassette. Plasmids were transformed into a *SHE2* deletion strain, and expression levels were estimated via Western blotting using an anti-HA antibody.

In Situ Hybridization

Yeast cells were grown to mid-log phase and processed for in situ hybridization as described in Long et al. (2000) using a pool of Cy3-labeled oligonucleotides against *ASH1* mRNA.

RNA Binding Experiments

Radiolabeled E3 zip code element of *ASH1* mRNA was added to serial dilutions of full-length She2p (wild-type or mutant forms) in 200 mM KoAc, 50 mM Tris (pH 7.4), 5 mM MgOAc, 1 mM DTT, and 30 ug/ml yeast tRNA, as described in Farina et al. (2003). Radioactivity retained on a nitrocellulose filter was measured. Best fit analyses and calculation of equilibrium dissociation constants from a plot of the fraction of bound RNA versus protein concentration were performed using the Langmuir Isotherm, assuming a single binding site. For all She2p variants, three independent experiments for each of at least six different dilutions were performed.

Comparative RNA binding experiments for wild-type She2p were also performed with 0.25, 0.5, 1, and 5 mM MgOAc, showing no significant differences in their respective equilibrium dissociation constants (data not shown). For stoichiometric RNA binding experiments, 100 nM wild-type She2p was titrated against near-stoichiometric concentrations of E3 zip code element up to a total of 2.5-fold excess. The binding buffer used in this study contained 1 mM MgOAc. The transcript used for RNA binding studies consists of the E3 zip code element (capital letters) and vector sequence (small letters): 5′-gggcgaauucgagcucgguaccGAGACAGUAGAGAAUUGAUACAUGGAUAACUGAAUCUCUUUCAACUAAUAAGAGACAUUAUCACGAAACAAUUGUACAUUUCUCUCCUUGUCUGUGCUAAAUAAACUACAAAUAAAAAcugcaggcaygca-3′.

Acknowledgments

Use of the Advanced Photon Source was supported by the U.S. Department of Energy, Office of Science, Office of Basic Energy Sciences, under Contract No. W-31-109-Eng-38. Use of the SGX Collaborative Access Team (SGX-CAT) beamline facilities at Sector 31 of the Advanced Photon Source was provided by Structural GenomiX, Inc., which constructed and operates the facility. We are grateful to Dr. J.B. Bonanno for technical support and advice during data analyses and structure determination; to Xiuhua Meng for excellent support with filter binding experiments; to Dr. A.K. Padyana for help during structure determination; to Dr. S. Wasserman for assistance with X-ray diffraction data collection; to Dr. Brian Noland for assistance with Circular Dichroism measurements; and to K. Bain, M. Buchanan, D. Phanstiel, Dr. X. Gao, M. Maletich, M. Riedy, and Dr. X. Zhao for technical support. We also thank Drs. S. Antonysamy, R.C. Deo, C. Groft, C. Kissinger, H.A. Lewis, G. Louie, J. Marcotrigiano, A.K. Padyana, F. Park, and X. Zhao for many useful discussions. We are thankful to J. Kosh and Dr. C. Stamper at Keck Biophysics Facility of Northwestern University (IL) and Dr. B. Demeler at The University of Texas Health Science Center at San Antonio (TX) for help with analytical ultracentrifugation. D.N. was supported by a long-term fellowship of the Human Frontiers Science Program (HFSP) and an "Otto-Hahn-Medaille" fellowship of the Max-Planck Society. S.K.B. was an investigator in the Howard Hughes Medical Institute. This work was supported by NIGMS grant GM61262 (S.K.B.) and NIGMS grant GM57071 (R.H.S.).

Received: July 19, 2004
Revised: September 20, 2004
Accepted: September 30, 2004
Published: November 11, 2004

References

Bertrand, E., Chartrand, P., Schaefer, M., Shenoy, S.M., Singer, R.H., and Long, R.M. (1998). Localization of *ASH1* mRNA particles in living yeast. Mol. Cell *2*, 437–445.

Bobola, N., Jansen, R.P., Shin, T.H., and Nasmyth, K. (1996). Asymmetric accumulation of Ash1p in postanaphase nuclei depends on

a myosin and restricts yeast mating-type switching to mother cells. Cell *84*, 699–709.

Böhl, F., Kruse, C., Frank, A., Ferring, D., and Jansen, R.P. (2000). She2p, a novel RNA-binding protein tethers *ASH1* mRNA to the Myo4p myosin motor via She3p. EMBO J. *19*, 5514–5524.

Brünger, A.T. (1992). Free R value: a novel statistical quantity for assessing the accuracy of crystal structures. Nature *355*, 472–475.

Chartrand, P., Meng, X.H., Singer, R.H., and Long, R.M. (1999). Structural elements required for the localization of *ASH1* mRNA and of a green fluorescent protein reporter particle in vivo. Curr. Biol. *9*, 333–336.

Chartrand, P., Singer, R.H., and Long, R.M. (2001). RNP localization and transport in yeast. Annu. Rev. Cell Dev. Biol. *17*, 297–310.

Chartrand, P., Meng, X.H., Hüttelmaier, S., Donato, D., and Singer, R.H. (2002). Asymmetric sorting of ash1p in yeast results from inhibition of translation by localization elements in the mRNA. Mol. Cell *10*, 1319–1330.

Cohen, S.L., and Chait, B.T. (2001). Mass spectrometry as a tool for protein crystallography. Annu. Rev. Biophys. Biomol. Struct. *30*, 67–85.

Collaborative Computational Project. (1994). The CCP4 suite: programs for protein crystallography. Acta Crystallogr. D. Biol. Crystallogr. *50*, 760–763.

Conte, L.L., Chothia, C., and Janin, J. (1999). The atomic structure of protein-protein recognition sites. J. Mol. Biol. *285*, 2177–2198.

Darzacq, X., Powrie, E., Gu, W., Singer, R.H., and Zenklusen, D. (2003). RNA asymmetric distribution and daughter/mother differentiation in yeast. Curr. Opin. Microbiol. *6*, 614–620.

Dasgupta, S., Iyer, G.H., Bryant, S.H., Lawrence, C.E., and Bell, J.A. (1997). Extent and nature of contacts between protein molecules in crystal lattices and between subunits of protein oligomers. Proteins *28*, 494–514.

Dietrich, F.S., Voegeli, S., Brachat, S., Lerch, A., Gates, K., Steiner, S., Mohr, C., Pohlmann, R., Luedi, P., Choi, S., et al. (2004). The *Ashbya gossypii* genome as a tool for mapping the ancient *Saccharomyces cerevisiae* genome. Science *304*, 304–307.

Ding, B., Itaya, A., and Qi, Y. (2003). Symplasmic protein and RNA traffic: regulatory points and regulatory factors. Curr. Opin. Plant Biol. *6*, 596–602.

Dreyfuss, G., Kim, V.N., and Kataoka, N. (2002). Messenger-RNA-binding proteins and the messages they carry. Nat. Rev. Mol. Cell Biol. *3*, 195–205.

Estevez, M., Skarda, J., Spencer, J., Banaszak, L., and Weaver, T.M. (2002). X-ray crystallographic and kinetic correlation of a clinically observed human fumarase mutation. Protein Sci. *11*, 1552–1557.

Farina, K.L., and Singer, R.H. (2002). The nuclear connection in RNA transport and localization. Trends Cell Biol. *12*, 466–472.

Farina, K.L., Hüttelmaier, S., Musunuru, K., Darnell, R., and Singer, R.H. (2003). Two ZBP1 KH domains facilitate beta-actin mRNA localization, granule formation, and cytoskeletal attachment. J. Cell Biol. *160*, 77–87.

Ferré-D'Amaré, A.R., and Burley, S.K. (1997). Dynamic light scattering in evaluating crystallizability of macromolecules. Methods Enzymol. *276*, 157–166.

Ghaemmaghami, S., Huh, W.K., Bower, K., Howson, R.W., Belle, A., Dephoure, N., O'Shea, E.K., and Weissman, J.S. (2003). Global analysis of protein expression in yeast. Nature *425*, 737–741.

Gonsalvez, G.B., Lehmann, K.A., Ho, D.K., Stanitsa, E.S., Williamson, J.R., and Long, R.M. (2003). RNA-protein interactions promote asymmetric sorting of the *ASH1* mRNA ribonucleoprotein complex. RNA *9*, 1383–1399.

Gonzalez, I., Buonomo, S.B., Nasmyth, K., and von Ahsen, U. (1999). *ASH1* mRNA localization in yeast involves multiple secondary structural elements and Ash1 protein translation. Curr. Biol. *9*, 337–340.

Gu, W., Deng, Y., Zenklusen, D., and Singer, R.H. (2004). A new yeast PUF family protein, Puf6p, represses *ASH1* mRNA translation and is required for its localization. Genes Dev. *18*, 1452–1465.

Holm, L., and Sander, C. (1998). Touring protein fold space with Dali/FSSP. Nucleic Acids Res. *26*, 316–319.

Jansen, R.P., Dowzer, C., Michaelis, C., Galova, M., and Nasmyth, K. (1996). Mother cell-specific HO expression in budding yeast depends on the unconventional myosin myo4p and other cytoplasmic proteins. Cell *84*, 687–697.

Ke, H. (1997). Overview of Isomorphous Replacement Phasing. In Methods in Enzymology, C.W. Carter and R.M. Sweet, eds. (San Diego, CA: Academic Press), pp. 448–461.

Kellis, M., Birren, B.W., and Lander, E.S. (2004). Proof and evolutionary analysis of ancient genome duplication in the yeast *Saccharomyces cerevisiae*. Nature *428*, 617–624.

Kloc, M., Zearfoss, N.R., and Etkin, L.D. (2002). Mechanisms of subcellular mRNA localization. Cell *108*, 533–544.

Kruse, C., Jaedicke, A., Beaudouin, J., Böhl, F., Ferring, D., Güttler, T., Ellenberg, J., and Jansen, R.P. (2002). Ribonucleoprotein-dependent localization of the yeast class V myosin Myo4p. J. Cell Biol. *159*, 971–982.

Laskowski, R.J., MacArthur, M.W., Moss, D.S., and Thornton, J.M. (1993). PROCHECK: a program to check stereochemical quality of protein structures. J. Appl. Crystallogr. *26*, 283–290.

Levitt, D.G. (2001). A new software routine that automates the fitting of protein X-ray crystallographic electron-density maps. Acta Crystallogr. D. Biol. Crystallogr. *57*, 1013–1019.

Long, R.M., Singer, R.H., Meng, X., Gonzalez, I., Nasmyth, K., and Jansen, R.P. (1997). Mating type switching in yeast controlled by asymmetric localization of *ASH1* mRNA. Science *277*, 383–387.

Long, R.M., Gu, W., Lorimer, E., Singer, R.H., and Chartrand, P. (2000). She2p is a novel RNA-binding protein that recruits the Myo4p-She3p complex to *ASH1* mRNA. EMBO J. *19*, 6592–6601.

Lopez de Heredia, M., and Jansen, R.P. (2004). mRNA localization and the cytoskeleton. Curr. Opin. Cell Biol. *16*, 80–85.

Mohr, E., and Richter, D. (2001). Messenger RNA on the move: implications for cell polarity. Int. J. Biochem. Cell Biol. *33*, 669–679.

Münchow, S., Sauter, C., and Jansen, R.P. (1999). Association of the class V myosin Myo4p with a localised messenger RNA in budding yeast depends on She proteins. J. Cell Sci. *112*, 1511–1518.

Nadassy, K., Wodak, S.J., and Janin, J. (1999). Structural features of protein-nucleic acid recognition sites. Biochemistry *38*, 1999–2017.

Nagai, K. (1996). RNA-protein complexes. Curr. Opin. Struct. Biol. *6*, 53–61.

Nicholls, A., Sharp, K., and Honig, B. (1991). Protein folding and association: insights from the interfacial and thermodynamic properties of hydrocarbons. Proteins *11*, 281–296.

Nicholls, A., Bharadwaj, R., and Honig, B. (1993). GRASP: Graphical Representation and Analysis of Surface Properties. Biophys. J. *64*, A116.

Otwinowski, Z., and Minor, W. (1997). Processing of X-ray diffraction data collected in oscillation mode. In Methods of Enzymology, C.W. Carter and R.M. Sweet, eds. (San Diego, CA: Academic Press), pp. 307–326.

Pieper, U., Eswar, N., Braberg, H., Madhusudhan, M.S., Davis, F.P., Stuart, A.C., Mirkovic, N., Rossi, A., Marti-Renom, M.A., Fiser, A., et al. (2004). MODBASE, a database of annotated comparative protein structure models, and associated resources. Nucleic Acids Res. *32*, D217–D222.

Reck-Peterson, S.L., Tyska, M.J., Novick, P.J., and Mooseker, M.S. (2001). The yeast class V myosins, Myo2p and Myo4p, are nonprocessive actin-based motors. J. Cell Biol. *153*, 1121–1126.

Sander, C., and Schneider, R. (1991). Database of homology-derived protein structures and the structural meaning of sequence alignment. Proteins *9*, 56–58.

Sil, A., and Herskowitz, I. (1996). Identification of asymmetrically localized determinant, Ash1p, required for lineage-specific transcription of the yeast HO gene. Cell *84*, 711–722.

Steward, O., and Worley, P. (2001). Localization of mRNAs at synaptic sites on dendrites. Results Probl. Cell Differ. *34*, 1–26.

St Johnston, D. (1995). The intracellular localization of messenger RNAs. Cell *81*, 161–170.

Takizawa, P.A., and Vale, R.D. (2000). The myosin motor, Myo4p, binds *Ash1* mRNA via the adapter protein, She3p. Proc. Natl. Acad. Sci. USA *97*, 5273–5278.

Takizawa, P.A., Sil, A., Swedlow, J.R., Herskowitz, I., and Vale, R.D. (1997). Actin-dependent localization of an RNA encoding a cell-fate determinant in yeast. Nature *389*, 90–93.

Tekotte, H., and Davis, I. (2002). Intracellular mRNA localization: motors move messages. Trends Genet. *18*, 636–642.

Thompson, J.D., Gibson, T.J., Plewniak, F., Jeanmougin, F., and Higgins, D.G. (1997). The CLUSTAL_X windows interface: flexible strategies for multiple sequence alignment aided by quality analysis tools. Nucleic Acids Res. *25*, 4876–4882.

Tyson, C.B., Lord, P.G., and Wheals, A.E. (1979). Dependency of size of *Saccharomyces cerevisiae* cells on growth rate. J. Bacteriol. *138*, 92–98.

Vale, R.D. (2003). The molecular motor toolbox for intracellular transport. Cell *112*, 467–480.

Vinkemeier, U., Cohen, S.L., Moarefi, I., Chait, B.T., Kuriyan, J., and Darnell, J.E., Jr. (1996). DNA binding of *in vitro* activated Stat1 alpha, Stat1 beta and truncated Stat1: interaction between NH2-terminal domains stabilizes binding of two dimers to tandem DNA sites. EMBO J. *15*, 5616–5626.

Weaver, T.M., Levitt, D.G., Donnelly, M.I., Stevens, P.P., and Banaszak, L.J. (1995). The multisubunit active site of fumarase C from *Escherichia coli*. Nat. Struct. Biol. *2*, 654–662.

Weeks, C.M., and Miller, R. (1999). The design and implementation of *SnB* V2.0. J. Appl. Crystallogr. *32*, 120–124.

Wickens, M., Goodwin, E.B., Kimble, J., Strickland, S., and Hentze, M.W. (2000). Translational Control of Developmental Decisions. In Translational Control of Gene Expression, N. Sonenberg, J.W.B. Hershey, and M.B. Mathews, eds. (Cold Spring Harbor, NY: Cold Spring Harbor Laboratory Press), pp. 295–370.

Woods, S.A., Miles, J.S., Roberts, R.E., and Guest, J.R. (1986). Structural and functional relationships between fumarase and aspartase. Nucleotide sequences of the fumarase (fumC) and aspartase (aspA) genes of *Escherichia coli* K12. Biochem. J. *237*, 547–557.

Zucker, M. (1998). On finding all suboptimal foldings of an RNA molecule. Science *244*, 48–52.

Accession Numbers

The refined atomic coordinates and X-ray structure factors for She2p have been deposited in the Protein Data Bank under ID code 1XLY.